Reactions of an Organoruthenium Anticancer Complex with 2-Mercaptobenzanilide - a Model for the Active-site Cysteine of Protein Tyrosine Phosphatase 1B

Yumiao Han,[a,b] Qun Luo, [a,b] Xiang Hao, [b] Xianchan Li, [a,b] Fuyi Wang, [*a,b] Wenbing Hu, [a,b] Kui Wu, [a,b] Shuang Lü, [a,b] Peter J. Sadler[*c]

Received (in XXX, XXX) Xth XXXXXXXXX 200X, Accepted Xth XXXXXXXXX 200X

DOI: 10.1039/b000000x

Abstract: The organometallic anticancer complex [(η^6-cymene)Ru(en)Cl]PF_6 (**1**, en = ethylenediamine) readily reacts with thiols and forms stable sulfenate/sulfinate adducts which may be important for its biological activity. Protein tyrosine phosphatase 1B (PTP1B), a therapeutic target, contains a catalytic cysteinyl thiol and is involved in the regulation of insulin signaling and the balance of protein tyrosine kinase activity. On oxidation, the catalytic Cys215 can form an unusual sulfenyl-amide intermediate which can subsequently be reduced by glutathione. Here we study reactions of **1** with 2-mercaptobenzanilide, **2**, a chemical model for the active site of PTP1B. We have characterized crystallographically compound **2** and its oxidized sulfenyl-amide derivative 2-phenyl-1,2-benzisothiazol-3(2H)-one (**4**) which shows a close structural similarity to the sulfenyl-amide in oxidized PTP1B. At pH 7.4 and 5.3, **1** reacted with **2**, affording a mono-ruthenium thiolato complex [(η^6-cym)Ru(en)(S-RS)]$^+$ (**7**$^+$, R = (C_6H_5)CONH(C_6H_5)) and a triply-S-bridged thiolato complex [((η^6-cym)Ru)$_2$(μ-S-RS)$_3$]$^+$ (**8**$^+$), respectively. Coordination of Ru to the S atom in **7** allows formation of a strong H-bond (2.02 Å) between the en-NH and the carbonyl oxygen. To assess the possible effect of ruthenium coordination on the redox regulation of PTP1B, reactions of these thiolato products with H_2O_2 and/or GSH were investigated, demonstrating that coordination to Ru largely retards both the oxidation (deactivation) of the thiol in compound **2** by H_2O_2 and the subsequent reduction (reactivation) of the sulfenyl-amide by GSH, implying that the inhibition of

complex **1** on PTP1B (IC_{50} of 19 μM) may be attributed to coordination to its catalytic cysteine.

Introduction

Organometallic ruthenium(II) complexes are a family of ruthenium(II) compounds of interest as potential antitumor agents,[1-9] and for the type [(η^6-arene)Ru(YZ)(X)][PF_6], where X is a halide and YZ is a chelating diamine such as ethylenediamine (en), have *in vitro* and *in vivo* anticancer activity, including cisplatin-resistant cell lines.[10-13] The arene ligand occupies three coordination sites in these pseudo-octahedral complexes and stabilizes Ru in its +2 oxidation state.[14] For the family of chlorido en complexes [(η^6-arene)Ru(en)Cl][PF_6], the cytotoxicity increases with the size of the coordinated arene, and the cytotoxicity of the *p*-cymene complex against human ovarian cancer cell line A2780 is comparable to that of carboplatin.[10, 12] DNA is a potential target for these ruthenium(II) arene complexes, most of which bind selectively to N7 of guanine.[15-20] However, these organometallic ruthenium anticancer complexes also have a high affinity for the thiolate sulfur in cysteine,[21] glutathione[22] and human albumin,[23, 24] and Ru-S coordination can induce the oxidation of thiolates to sulfenates or sulfinates,[22-24] and subsequently stabilizes the sulfenato ligands[23, 25] which as free ligands are often unstable and highly reactive.[26, 27] Moreover, glutathione was shown to be kinetically competitive with cGMP for coordination with the ruthenium biphenyl complex, and the oxidation of coordinated glutathione in the resulting thiolato ruthenium complex to sulfenate ligand appears to provide a facile route for displacement of S-bound glutathione by G N7.[22]

The protein tyrosine phosphatase 1B (PTP1B) negatively regulates insulin signaling by dephosphorylating the phosphorylated tyrosine residues of the insulin receptor kinase, and is involved in balancing protein tyrosine kinase (PTK) activity as part of normal growth-regulation pathways.[28-32] Increasing interest is focused on PTP1B as an effective target for both anti-diabetes/obesity drug discovery[33-35] and the

treatment of human breast and ovarian cancers, a significant subset of which, especially HER2/Neu HER2(+) tumors, overexpress PTP1B.[29, 30, 36] The catalytic site residue Cys215 plays a central role in modulating the activity of PTP1B, and is a key feature in the deactivation/reactivation pathway involving the formation and the subsequent reduction of a sulfenyl-amide intermediate mediated by the endogenous signaling molecules hydrogen peroxide (H_2O_2) and glutathione (GSH), respectively.[37-40] This intriguing behavior of PTP1B led us to explore whether ruthenium arene anticancer complexes coordinate to the catalytic thiol of PTP1B and inhibit enzyme activity *via* the induced oxidation of thiol to sulfinate/sulfenate and the subsequent stabilization of the sulfenate.

Indeed, in a preliminary study, we found that the ruthenium arene anticancer complex $[(\eta^6\text{-}p\text{-cym})Ru(en)Cl]PF_6$ (**1**, cym = cymene) is inhibitory towards PTP1B with an IC_{50} of 19 μM.[41] In the present work, therefore, the thiol 2-mercaptobenanilide (**2**), and the product of H_2O_2-oxidation, the sulfenyl-amide derivative 2-phenyl-1,2-benzisothiazol-3(2*H*)-one, have been synthesized and characterized crystallographically for first time to mimic the interactions between complex **1** and the catalytic cysteine site of PTP1B. The aromatic thiol compound 2-mercaptobenanilide is an established chemical model for the redox regulation of PTP1B, including the formation of the sulfenyl-amide intermediate in the presence of H_2O_2 and GSH-mediated reactivation of the inert intermediate,[38, 39] because the ortho-substituted benzene scaffold provides a good model for the proximity of the amide and the thiol group at the active site of PTP1B[37-40] which is not readily duplicated by aliphatic thiolates. Interactions between complex **1** and the model compound **2** are then investigated by mass spectrometry (MS) coupled with high performance liquid chromatography (HPLC). Redox reactions of the resulting mono- and di-nuclear thiolato products, which were both characterized by X-ray diffraction analysis, were studied to mimic the effect of ruthenium coordination on the inactivation and reactivation of PTP1B.

Results

Synthesis and crystallographic characterization of 2-mercaptobenzanilide:

The model compound 2-mercaptobenzanilide (**2**) was synthesized following the procedure described in the literature,[38, 39, 42] and crystallized from a saturated solution in methanol. The X-ray structure and atom numbering scheme are depicted in Figure 1a, crystallographic data are listed in Table 1, and selected bond lengths and angles in Table 2. As expected, the distance between the sulfur atom (S1) of the thiol and the nitrogen atom (N1) of the amide in compound **2** (3.8 Å) is similar to that (3.5 Å) between the thiol group of Cys215 and the amide N of Ser216 at the active site of PTP1B.[37, 40, 43]

To mimic the redox regulation of PTP1B, compound **2** (1 mM) was incubated with 1.4 mol equiv. of H_2O_2 in 50 mM sodium phosphate buffer (pH 7.4) containing 30% MeCN, which was used to increase the solubility of compound **2** in the reaction mixture, at 298 K. This reaction immediately gave rise to a product as detected by HPLC analysis (peak b in Figure 2a). Compound **2** (peak a in the HPLC traces) almost disappeared after 0.5 h of reaction, accompanied by the formation of a second product, corresponding to HPLC peak c with the same retention time (11.0 min) as peak a, as evidenced by their different UV-Vis spectra recorded by the DAD UV-Vis detector (Figure 2b). One hour later, the reaction afforded two further products (peaks d and e), and the peaks c, d and e all increased in intensity until 24 h (Figure 2a). The subsequent ESI-MS analysis of all the HPLC fractions gave rise to singly-charged ion peaks at *m/z* (the most abundant isotope mass-to-charge ratio) of 230.02, 457.01, 228.00, 278.02 and 244.01 for peaks a, b, c, d, and e (Table 3 and Figure S1), assignable to compound **2**, its oxidized derivatives disulfide compound **3**, sulfenyl-amide compound **4**, sulfonic acid **5** and sulfinyl-amide compound **6** (Scheme 1), respectively. The mass spectra (Figure S1) of peaks a and c showed that there is a 2 Da difference between the masses of species contained in these two peaks, indicating that this reaction afforded the expected sulfenyl-amide compound (**4**)

which is analogous to the sulfenyl-amide intermediate formed after the H_2O_2-mediated inactivation of PTP1B.[37, 39, 40]

We were also successful in crystallizing the sulfenyl-amide compound 2-phenyl-1,2-benzisothiazol-3(2*H*)-one (**4**) from a saturated ethanol solution. The X-ray structure is shown in Figure 1b, and the crystallographic data and the selected bond lengths and angles are listed in Tables 1 and 2, respectively. Except for the formation of the new S1-N1 bond, there is little change in other bond lengths compared to **2**. In compound **4**, it is notable that the C1-N1-S1-C7-C2 ring is almost coplanar with the benzene ring (dihedral angle < 3°).

Then the purified sulfenyl-amide compound **4** (1 mM) was incubated with 10 equiv. mol of GSH in 50 mM phosphate buffer (pH = 7.4) containing 30% MeCN at 298 K. The reaction was complete within 5 minutes and compound **4** was completely reduced back to the model compound **2** according to the HPLC analysis (data not shown). This reaction is the direct analog to the GSH-mediated reactivation of the sulfenyl-amide intermediate formed by the catalytic thiol group of the enzyme PTP1B.[37, 39, 40]

Reaction of [(η^6-cym)Ru(en)Cl]PF_6 (1) with 2-mercaptobenzanilide (2):

To mimic the interaction of organometallic ruthenium anticancer complexes with PTP1B, [(η^6-cym)Ru(en)Cl]PF_6 (**1**, 5 mM) was treated with 1 mol equiv. of compound **2** in 50 mM phosphate buffer (pH 7.4, containing 30% CH_3CN). In order to minimize the content of O_2, the solutions were purged by bubbling with argon before and after mixing. The reaction reached equilibrium at 4 h, and the main product was identified by ESI-MS to be a thiolato ruthenium complex (Scheme 2), as indicated by the singly-charged ion peak at *m/z* 523.32 corresponding to [(η^6-cym)Ru(en)(RS)]$^+$ (**7**$^+$) (R = (C_6H_5)CONH(C_6H_5), calculated(calc.) *m/z* 523.32 for **7**$^+$**)** as shown in Figure S2. Even in the presence of a 10-fold molar excess of GSH, the reaction of complex **1** with compound **2** still afforded the mono-ruthenium thiolato complex **7** containing the 2-mercaptobenzanilide ligand as the main product, and no

glutathione thiolato complex was detectable in the reaction mixture incubated at 298 K for 48 h (Figure S3).

The thiolato compound **7** was precipitated by adding NH_4PF_6 to the equilibrium reaction mixture containing 5 mM **1** with one mol equiv **2** and recrystallized from dichloromethane/ether. Crystals suitable for X-ray analysis were obtained by slow evaporation of a dichloromethane/ether solution at 253 K. The crystallographic data for **7** are listed in Table 1, and selected bond lengths and angles in Table 4. As shown in Figure 3, the coordination of Ru to the sulfur atom in **2** allows the formation of an H-bond between the NH of the en ligand and the carbonyl oxygen with a bond (NH···OC) length of 2.02 Å (Figure S4), indicative of a strong H-bonding. The Ru-S bond length (2.4059(9) Å) is slightly longer than that in the thiolato compound [(η^6-*p*-cymene)Ru(en)(*S*-C_6H_6)]I.[25] The thiolato complex **7** is soluble and stable in aqueous solution; ca. 94 % of **7** remained intact after 60 h incubation in phosphate buffer at 298 K (Figure S5). However, at pH 5.3, nearly 15% of **7** hydrolyzed after 60 h incubation. Notably, the hydrolysis occurred *via* the dissociation of the en ligand instead of the thiolate ligand, giving rise to a di-aqua adduct [(η^6-cym)Ru(*S*-(C_6H_5)CONH(C_6H_5)S)(H_2O)$_2$]$^+$ (**9**) as shown in Scheme 3 and Figure S5.

The pK_a of the thiol of the model compound **2** is reported to be 5.7, similar to that of the active-site thiol in PTP1B (5.6).[39] The reaction of the protonated ligand **2** with the ruthenium complex was also investigated in 50 mM phosphate buffer containing 50% methanol at pH 5.3 which is similar to the pH in endosomes (5-6).[44] Interestingly, this reaction afforded a di-ruthenium thiolato complex (Scheme 2) as indicated by a doubly-charged ion peak at *m/z* 1156.22 assignable to the cation [((η^6-cym)Ru)$_2$(RS)$_3$]$^+$ (**8**$^+$) (R = (C_6H_5)CONH(C_6H_5), calc. *m/z* 1156.32 for **8**$^+$) in the mass spectrum of the product (Figure S2). This di-ruthenium thiolato complex was also precipitated by a similar procedure described above, washed with diethyl ether, and dried in vacuum. The crude mixture was then purified by flash column chromatography eluting with dichloromethane/methanol (11:0.2). Slow evaporation

of the dichloromethane/methanol solvent gave rise to red crystals suitable for X-ray diffraction studies. The crystallographic data are listed in Table 1, and selected bond lengths and angles in Table 3. These results show that the di-nuclear product is a triply-S-bridged thiolato complex $[((\eta^6\text{-cym})Ru)_2(\mu\text{-}S\text{-}RS)_3]PF_6$ (Figure 4), which adopts a "sandwich" configuration. It is notable that there is an intermolecular H-bond between the amide N3-H and the adjacent sulfur atom S3 in the thiolato ligand (Figure S5) with the N-H···S bond length of 2.51 Å whereas no H-bond is observed between the amide proton and the sulfur atom in other two thiolato ligands. The bond lengths of the three thiolato ligands and the six Ru-S bonds in complex **8** differ slightly from each another, while the angles of the three thiolato ligands are markedly different from each another (Table 4).

Reactions of thiolato adduct 7 with H_2O_2 and GSH:

To provide a model for the H_2O_2-mediated oxidation and the subsequent GSH-mediated reduction, the thiolato ruthenium complex **7** (1 mM) was incubated with 1.4 mol equiv. of H_2O_2 in phosphate buffer (pH =7.4, containing 30% MeCN) at 298 K, and the reaction was followed by HPLC coupled with ESI-MS. The HPLC time-course (Figure 5a) showed a minor product (peak c) after ca. 0.5 h, and then other two adducts (peaks h and e) after 1.5 h. Up to 7.5 h, peaks c, h and e slowly increased in intensity, but no obvious changes in intensity were observed for all three peaks after 12 h (Figure 5a).

The subsequent ESI-MS analysis identified fractions c and e as containing the oxidized derivatives **4** (sulfenyl-amide) and **6** (sulfinyl-amide), respectively, as indicated by the singly-charged ion peaks at *m/z* 244.01 and 228.00 (Figure S6, Table 3). The inset in Figure 5a shows peak h having a shoulder, suggesting that this peak contains a mixture of products formed from the oxidation of complex **7**, as evidenced by distinct UV-Vis spectra of fractions eluting at 5.00 and 5.05 min (Figure S7). The mass spectra of these fractions (Figure S6, Table 3) show two singly-charged ion peaks at *m/z* 422.16 and 463.17, assignable to the fragment ion $\{Ru^{II}(en)(RS(O)_2)]^+$

(R = $(C_6H_5)CONH(C_6H_5)$) of sulfinato Ru(II) arene complex $[(\eta^6\text{-cym})Ru^{II}(en)(RS(O)_2)]^+$ (**10**) (calc.*m/z* 422.16 for $\{[(\eta^6\text{-cym})Ru^{II}(en)(RS(O)_2)] - (\eta^6\text{-cym})\}^+$) and a fragment ion $\{(\eta^6\text{-cym})Ru^{III}(RS)\}^{2+}$ of the thiolato Ru(III) arene adduct $[(\eta^6\text{-cym})Ru^{III}(en)(RS)]^{2+}$ (**11**) (calc. *m/z* 463.17 for $\{[(\eta^6\text{-cym})Ru^{III}(en)(RS)] – en – H\}^+$), respectively. After 72 h of reaction with 1.4 mol equiv. H_2O_2, ca. 52% of complex **7** remain intact.

To mimic the effect of ruthenium coordination on the redox regulation of the catalytic thiol group in PTP1B, the mono-ruthenium thiolato complex $[(\eta^6\text{-cym})Ru(en)(RS)]^+$ (R = $(C_6H_5)CONH(C_6H_5)$) (**7**) was first allowed to react with 1.4 mol equiv. H_2O_2 in phosphate buffer (pH 7.4) for 24 h, and then 10 mol equiv. GSH was added to the reaction mixture after removing excess H_2O_2 by addition of catalase (260 units mL^{-1}). The resulting mixture was incubated at 298 K and monitored by HPLC assay. As shown in Figure 5b, the sulfenyl-amide compound **4** (peak c) resulting from the oxidation of the dissociated thiolato ligand in **7** by H_2O_2 was quickly reduced by GSH back to its initial form, i.e. the thiol compound **2** (peak a in Figure 5b) which increased in concentration until 72 h. However, the sulfinato Ru(II) complex **10** and the thiolato Ru(III) complex **11** (peak h) resulting from the oxidation of complex **7**, as well as the sulfinyl-amide compound **6** resulting from the oxidation of dissociated thiolate ligand in **7** by H_2O_2, remain intact in the presence of a 10-fold excess of GSH. The triply-glutathione-bridged diruthenium complex **13** (peak i) and a mixed-disulfide compound GS-S$(C_6H_6)CONH(C_6H_6)$ (**17,** peak j), as indicated by the mass spectra of these fractions (Table 3, Figure S8), appeared in the HPLC chromatogram (Figure 5b) after 24 h of reaction.

At pH 5.3 thiolato complex **7** reacted with H_2O_2 much more extensively than at 7.4. This reaction gave rise to a significant amount of the sulfenyl-amide compound **4** (peak c in Figure 6) which resulted from the oxidation of the dissociated thiolate ligand from **7,** and a significant amount of the sulfinato Ru(II) complex **10** and the thiolato Ru(III) complex **11** (peak h in Figure 6). Meanwhile, the diaqua adduct $[(\eta^6\text{-cym})Ru(RS)(H_2O)_2]^+$ (**9**, R = $(C_6H_5)CONH(C_6H_5)$, peak g in Figure 6) formed

after the dissociation of the en ligand became detectable after 12 h reaction and increased in content until 72 h, when only 11.7% of **7** remained intact (Figure 6). Notably, due to its low extinction coefficient at 260 nm, the aqua Ru arene adduct $[(\eta^6\text{-cym})Ru(en)(H_2O)]^+$ (**1-H_2O**) resulting from the dissociation of the oxidized thiolate ligand was hardly detectable by HPLC (Figure 6). Combining the above results, the pathway for the reaction of complex **7** with H_2O_2 at pH 5.3 shown in Scheme 4 can be proposed.

To investigate whether the coordinated thiolate ligand in **7** can be released via direct substitution by GSH, the most abundant thiol-containing biomolecule inside cells, reaction of complex **7** (1 mM) with 10 mol equiv. of GSH in 50 mM phosphate buffer (pH =7.4, containing 30% MeCN at 298K) was also studied by HPLC coupled with ESI-MS. As shown in Figure 7a, during the early stages (< 0.5 h) no product was detectable by HPLC. A new HPLC peak (a in Figure 7a) appeared after 6.5 h of reaction and increased in intensity until 72 h. This was identified as the free thiol-containing compound **2** by subsequent MS analysis (Figure S10, Table 3). Meanwhile, after 12 h reaction, another product (peak k in Figure 7a) became detectable and was identified by MS (Figure S10) as the glutathione thiolato complex $[(\eta^6\text{-cym})Ru(en)(GS)]^+$ (**12**). After 72 h of reaction, nearly 43% of the thiolato ligand in **7** was substituted by GSH (Figure 7a), suggesting that GSH in 10-fold excess, can slowly displace the thiolato ligand from complex **7** (Scheme 5).

In weakly acidic solution (pH 5.3), as for the reaction of complex **7** with H_2O_2, the reaction of complex **7** with excess GSH also became extensive and complicated. After 6 h incubation, this reaction gave rise to a glutathione thiolato-bridged diruthenium product $[((\eta^6\text{-cym})Ru)_2(GS)_3]^+$ (**13**, appearing as peak i in Figure 7b) and a hetero-thiolato-bridged diruthenium complex $[((\eta^6\text{-cym})Ru)_2(GS)_2(RS)]^+$ (**14**, peak l in Figure 7b, R = $(C_6H_5)CONH(C_6H_5)$) as indicated by the doubly-charged ion peaks at *m/z* 695.64 (calc. *m/z* 695.64 for$\{[((\eta^6\text{- cym})Ru)_2(GS)_3] + H\}^{2+}$) and 656.89 (calc. *m/z* 656.89 for $\{[((\eta^6\text{-cym})Ru)_2(GS)_2(RS)] + H\}^{2+}$) (Figure S11), respectively, due to the dissociation of the en ligand and the substitution of the mercaptobenzanilide

ligand by GSH accompanied with the release of the mercaptobenzanilide ligand (peak a in Figure 7b). Six hours later, two other diruthenium products appeared and increased in concentration for 72 h. The MS results (Figure S11, Table 3) indicate that these two species are the hetero-thiolato-bridged adducts $[((\eta^6\text{-cym})Ru)_2(GS)(RS)_2]^+$ (**15**) and $[((\eta^6\text{-cym})Ru)_2(RS)_2(CHCO_2)(PO_3)]$ (**16**; the formate and phosphate ligands come from the HPLC solvents and the phosphate buffer, respectively). On the basis of HPLC peak areas, only ca. 13% of complex **7** remained intact after 72 h reaction with 10-fold excess GSH. Thus, the pathway for reaction of complex **7** with GSH at pH 5.3 shown in Scheme 5 can be proposed.

We also treated the fully characterized di-ruthenium thiolato adduct **8** with H_2O_2 and/or GSH by following the same procedures described above. No oxidized products with H_2O_2 or ligand-exchanged adducts with GSH were detectable after a 72 h reaction (data not shown), suggesting that this diruthenium thiolato complex is inert towards both GSH and H_2O_2.

Discussion

Ruthenium arene anticancer complexes $[(\eta^6\text{-arene})Ru(en)Cl]PF_6$ (arene = *p*-cymene (**1**) or biphenyl) can form strong adducts with the thiolate groups of cysteine,[21] glutathione[22, 45] and albumin.[23] Intriguingly, Ru-coordination can induce the oxidation of thiolato to sulfenates or sulfinates[22, 23, 45] in the presence of molecular oxygen. Ruthenium coordination stabilizes the sulfenato ligands.[22, 25] The free sulfenic acids are highly reactive and readily oxidized further to sulfinic or sulfonic acids.[26, 27] Such oxidation of Ru-SR bonds probably accompanied by protonation[46] leads to the ready displacement of the sulfur ligand by guanine N7[25] and DNA binding.[22] However, fate of the released sulfenic acid ligands is unknown.

Cysteine-215 in the catalytic site of the enzyme PTP1B undergoes redox regulation involving the formation of a sulfenyl-amide intermediate on oxidation by H_2O_2 and subsequent reduction with glutathione back to an active thiol.[37, 40] The formation of the sulfenyl-amide intermediate is thought to protect the thiol from

further oxidation to sulfinate or/and sulfonate which can irreversibly deactivate it.[37, 40] This unusual reaction prompted us to consider the possibility that ruthenium coordination to the catalytic cysteine of PTP1B might stabilize the sulfenate/sulfinate intermediate, prevent reactivation of the catalytic cysteine and thereby inhibit the enzyme. Indeed, in a preliminary study, ruthenium arene complex **1** was found to inhibit PTP1B with an IC_{50} of 19 μM.[41] In the present work, therefore, we have studied reactions of 2-mercaptobenanilide (**2**), a chemical model for Cys215 of PTP1B, with ruthenium anticancer complex **1,** including the formation and redox behavior of the resulting thiolato products.

Although compound **2** is well recognized as a chemical model of PTP1B, [38, 39] its X-ray crystal structure has not been previously reported. The crystallographic data obtained herein (Figure 1a, Table 2) show that the distance between the sulfur atom (S1) of the thiol and the nitrogen atom (N1) of the amide in compound **2** is similar to that between the sulfur atom in Cys215 and the nitrogen atom of the amide of Ser216 in PTP1B.[37, 40, 43] This is evidence that the ortho-substituted benzene scaffold of **2** indeed provides a good model for the proximity of the amide and the cysteine thiol group at the active site of PTP1B,[39] although the aromatic thiol in **2** may have a different reactivity towards ruthenium arene complexes compared to the aliphatic thiol[47] of the cysteine residue in the catalytic site of PTP1B.

Oxidation of compound **2** with H_2O_2 was fast, almost complete within 0.5 h. However, during this time, the main product was the disulfide compound **3** instead of the sulfenyl-amide compound **4** which formed after 0.5 h of reaction. This was accompanied by the formation of the sulfonic acid **5** and the sulfinyl-amide compound **6** (Figure 2a, Scheme 1). The sulfenyl-amide product **4** was separated from the reaction mixture and crystallographically characterized. Compound **4** is usually considered to be a good model for studying the GSH-mediated reactivation of the sulfenyl-amide intermediate of PTP1B. The X-ray structure of **4** (Figure 1b) shows the presence of the sulfenyl-amide (S1-N1) bond, with a bond length (1.7186(16) Å) similar to that of the sulfenyl-amide bond in oxidized PTP1B (1.7 Å).[40] Unlike the

puckered five-membered ring containing the sulfenyl-amide bond in the crowded catalytic site of PTP1B, the five-membered sulfenyl-amide ring in compound **4** is almost coplanar with the benzene ring (Figure 1b). However, this structural difference seemed to have little effect on the reduction of this sulfenyl-amide compound by GSH.[39] In the presence of a 10-fold excess of GSH, compound **4** was completely reduced back to its initial thiol form, i.e. compound **2**, within 5 min, directly analogous to the reactivation of the sulfenyl-amide intermediate during the redox regulation of PTP1B.[37, 40]

Having fully characterized the model compound **2** as well as its oxidation by H_2O_2 and subsequent reduction of the oxidized sulfenyl-amide product with GSH, we then studied reactions between compound **2** and the ruthenium complex **1**. At a 1:1 molar ratio, the reaction reached equilibrium within 4 h, affording the mono-ruthenium thiolato complex $[(\eta^6\text{-cym})Ru(en)(RS)]^+$ (**7**$^+$, R = $(C_6H_5)CONH(C_6H_5)$). Interestingly, in the presence of 10-fold excess of GSH, this mono-ruthenium thiolato complex was still the main product, indicating that complex **1** has a higher affinity for the thiol in **2** than for GSH. This might imply that PTP1B would form stronger adducts than GSH with ruthenium complex **1** in cells.

The crystallographic data (Table 4, Figure 3) show that the coordination of Ru with the sulfur atom in **2** allows the formation of a strong H-bond (NH···OC length: 2.02 Å, Figure S4) between the NH of en ligand and the carbonyl oxygen, which may account for the higher stability of the ruthenium adduct with compound **2** compared to GSH. The thiolato adduct with **2** (complex **7**) is soluble and stable in aqueous solution (pH 7.4), only 6% of **7** hydrolyzes after 60 h incubation at 298 K (Figure S5). However, at pH 5.3, nearly 15% of **7** hydrolyzed after 60 h incubation. Interestingly, the hydrolysis involved the displacement of the en ligand instead of the thiolate ligand, affording the di-aqua adduct **9** (Scheme 3, Figure S5). Sulfur-containing ligands such as cysteine and methionine are known to exhibit high *trans* effects in Pd(II)[48], Pt(II)[49] and Ru(II)[21] coordination chemistry, labilizing metal-N bonds in the *trans* position. On the other hand, at low pH the ethylenediamine (en) ligand is readily protonated,

making it a better leaving group, accounting for the dissociation of en from complex **7** in weakly acidic solutions. This *trans* effect imposed by S coordination to Ru was also observed in the reaction of complex **1** with the thiol compound **2**, and complex **7** with H_2O_2 or with GSH at pH 5.3. At pH 5.3, the majority of **2** is present in the RSH form (pK_a 5.7). When RSH attacks ruthenium in **1**, therefore, the proton can be transferred to the outgoing en,[46] leading to the formation of the final triply-thiolate-bridged diruthenium product $[((\eta^6\text{-cym})Ru)_2(RS)_3]^+$. For the reaction of complex **7** with H_2O_2 or GSH, as a consequence of the labilization of the en ligand in **7** by this *trans* effect, a significant amount of the diaqua adduct $[(\eta^6\text{-cym})Ru(RS)(H_2O)_2]^+$, the thiolato-bridged diruthenium product $[((\eta^6\text{-cym})Ru)_2(GS)_3]^+$ and the hetero-thiolato-bridged diruthenium complex $[((\eta^6\text{-cym})Ru)_2(GS)_2(RS)]^+$ (R = $(C_6H_5)CONH(C_6H_5)$) were formed (Figures 6 and 7b).

To mimic H_2O_2-mediated oxidation and the subsequent GSH-mediated reduction of the oxidized derivative of the catalytic thiol group coordinated to ruthenium of PTP1B, the redox behavior of the thiolato complex **7** was investigated and compared with that of the model compound **2**. During the early stages (< 0.5 h) of the reaction of **7** with H_2O_2 at pH 7.4, only a minor amount of the sulfenyl-amide compound **4** was observed. This is the oxidized derivative of the dissociated thiolato ligand which most probably resulted from the hydrolysis of complex **7** (*supra vide*). At a later stage (> 7.5 h), the sulfinyl-amide compound **6** (2-phenyl-1,2–benzisothiazol-3(2*H*)-one 1-oxide, Scheme 1) which also resulted from the oxidation of the dissociated thiolato ligand in **7** became detectable, accompanied by the formation of the Ru(II) sulfinato complex $[(\eta^6\text{-cym})Ru^{II}(en)(RS(O)_2)]^+$ (**10**) and a possible Ru(III) thiolato adduct $[(\eta^6\text{-cym})Ru^{III}(en)(RS)]^{2+}$ (**11**). The Ru(II) sulfinato complex **10** resulted from the oxidation of the thiolate ligand in **7**, and the Ru(III) thiolato complex **11** may be formed by oxidation of the Ru(II) in **7** (Figure S6, Table 3). Although there seems to be little precedent for such an oxidation, there is a report of the oxidation of the Ru(II) in the organoruthenium complex $[(\eta^6\text{-}C_6Me_6)Ru(tpdt)]$ (tpdt =

3-thiapentane-1,5-dithiolate) on reaction with Ph_2MCl_2 (M = Ge or Sn).[50] However, more than 50% of complex **7** remained intact after 72 h of reaction. At pH 5.3, due to the increase of the oxidation capacity of H_2O_2, more sulfinato and sulfenato Ru(II) complexes formed. The protonation of the sufenate ligand in **10** in turn labilizes the Ru-S(OH) bond,[46] probably accounting for the formation of more sulfenyl-amide compound **4** (Figure 6). However, there was still ca. 12% of **7** detected intact after reaction with excess of H_2O_2 for 72 h. These data imply that the coordinated thiolate ligand in **7** is much less reactive to H_2O_2 than the free thiol in **2** which was completely oxidized by 1.4 mol equiv H_2O_2 within 0.5 h.

When the mono-ruthenium thiolato complex **7** was first reacted with H_2O_2 at pH 7.4 for 24 h and then with excess of GSH (after removal of excess H_2O_2 by catalase), the small amount of sulfenyl-amide compound **4** resulting from the oxidation of the dissociated thiolate group from **7** was quickly reduced back to its initial form, compound **2**, accompanied with the formation of small amount of triply-glutathione-bridged diruthenium complex **13** and mixed disulfide compound GS-S(C_6H_6)CONH(C_6H_6) (**17**). The diruthenium complex **13** formed through the directly substitution of the thiolato ligand in **7** by GSH, leading to the further release of the thiolato ligand in **7** (Figure 5b) such that only ca. 10% of thiolato complex **7** was present in its initial form after 72 h reaction (Figure 7b). These data imply that under physiological conditions, intracellular GSH may activate the thiolate in **7** by displacing the thiolato ligand, though the ligand exchange is very slow (Figure 5).

At pH 5.3, the dissociation of the en ligand from **7** allowed formation of more glutathione-bridged diruthenium adduct **13** and mixed-thiolate-bridged adducts **14** and **15**. However, the amount of the free thiol compound **2** released from **7** did not increase compared with that formed at pH 7.4 (Figure 7).

Conclusions

The mercaptobenanilide compound **2** and its oxidized derivative the sulfenyl-amide compound **4** are models for species which form in the active site of the enzyme

PTP1B. Compounds **2** and **4** are characterized here for the first time by X-ray crystallography. The X-ray structures clearly indicate that the ortho-substituted benzene scaffold of **2** indeed provides a good model for the proximity of the amide and the cysteine thiol group at the active site of PTP1B. This is the key structure feature of the catalytic site leading to the formation of the sulfenyl-amide intermediate **4** which in turn protects the catalytic thiol from further oxidization into sulfinate, sulfonate, and can be reactivated by GSH-reduction back to thiol form. Obviously, a simple aliphatic thiol compound cannot duplicate this characteristic redox behavior.

Reaction of the ruthenium arene anticancer complex $[(\eta^6\text{-cym})Ru(en)Cl]PF_6$ (**1**) with **2** at pH 7.4 produced only the thiolato mono-ruthenium arene complex $[(\eta^6\text{-cymene})Ru(en)(RS)]^+$ (**7**, R = $(C_6H_5)CONH(C_6H_5)$) even in the presence of 10-fold excess of glutathione, implying that the ortho-substituted benzene enhances the reactivity of the thiol in **2** due to the formation of the strong H-bond between the NH of en ligand and the carbonyl oxygen. In contrast, at pH 5.3 the reaction of **1** with **2** gave rise to only a triply-S-bridged thiolato adduct $[((\eta^6\text{-cymene})Ru)_2(RS)_3]^+$ (**8**) due to the labilization of the en chelating ligand in **1**.

Further studies indicated that the coordination of ruthenium to the thiol sulfur of the model compound **2** largely retarded the oxidation (deactivation) by H_2O_2 of this sulfur to the sulfenyl-amide intermediate **4**. As a consequence, the reduction (reactivation) of the sulfenyl-amide intermediates by glutathione was significantly inhibited. The thiolate ligand $-S(C_6H_6)CONH(C_6H_6)$ in **7** is only slowly displaced by excess GSH and reactivated toward H_2O_2 oxidation. The activity of the thiolate in **7** towards H_2O_2 is much lower than that of the thiol in **2**. In addition the thiolate ligands in the triply-S-bridged diruthenium complex **8** are relatively inert towards both H_2O_2 and GSH. Such reactions may be implicated in the mechanism of action of this class of ruthenium arene anticancer complexes. With appropriate chemical modification to reduce their cytotoxicity, organometallic ruthenium complexes may have potential for treatment of diabetes as a family of novel PTP1B inhibitors.

Experimental

Materials and methods

[(η^6-cym)Ru(en)Cl]PF_6 (**1**) was synthesized as described previously.[11] $AgPF_6$ and trifluoroacetic acid (TFAH) were purchased from Alfa, acetonitrile (HPLC grade) from Merck, glutathione (GSH, reduced), hydrogen peroxide, 2-mercaptoberlzoic acid, aniline, sodium dihydrogen phosphate and NH_4PF_6 from Sinopharm Chemical Reagent Beijing Co., Ltd, *p*-nitrophenyl phosphate (*p*-NPP) from Sigma. The recombinant protein tyrosine phosphatase 1B (PTP1B) was a gift from Dr. Maolin Guo at University of Massachusetts Dartmouse.

Synthesis

2-Mercaptobenzanilide (2): Model compound **2** was synthesized following a reported procedure.[42] A suspension of o-mercaptoberlzoic acid and aniline at a molar ratio of 1:1 in chlorobenzene was heated to 343 K on an oil bath under argon, and small of amount of $PC1_3$ was gradually added during half an hour. After the addition was complete, the mixture was heated at reflux with stirring under Ar for 3 h. The resulting reaction mixture was filtered while hot, and the solvent evaporated to yield a white solid which was purified by flash column chromatography (10:1 EtOAc/hexane). Recrystallization from methanol gave white needle crystals suitable for X-ray diffraction studies. Yield: 0.87g (23.7 %). MS: *m/z* 230.02 [M^+].

2-Phenyl-1,2-benzisothiazol-3(2H)-one (4): Compound **4** was prepared according to a reported procedure.[51] To a well stirred mixture of benzamide (25 mg, 0.0975 mmol) and TFA (0.0225mL, 0.29 mmol) in 3 mL of CH_2Cl_2, a solution of phenyliodine(III)bis-(trifluoroacetate) (PIFA) (62.5 mg, 0.145 mmol) in 4.5 mL of CH_2Cl_2 was added. The resulting mixture was stirring at 273 K for 1 h, then filtered, and the solvent removed by evaporation. The crude mixture was purified by flash column chromatography (using dichloromethane) to afford the product as a white

solid, which was further purified by recrystallization from ethanol to give colorless block crystals suitable for X-ray diffraction studies. Yield: 8 mg (36 %). MS: *m/z* 228.00 [M^+].

HPLC-ESI-MS

Positive-ion electrospray ionisation mass spectra were obtained on a Micromass Q-TOF mass spectrometer (Waters) coupled to Agilent 1200 HPLC system using XDB-C18 column (4.6×150mm, 80Å, 5 µm, Agilent) with a flow rate of 1.0 mL min^{-1} and a splitting ratio of 1:10.. Mobile phases were A, water (purified using a MilliQ Reagent Water System) containing 0.1% TFA, and B, acetontrile containing 0.1% TFA. Gradient elution was achieved as follows (solvent B): 10% within 0 - 2 min; 10% – 42% over 2 – 3 min; 42% within 3 – 8 min; 42% – 68% over 8 – 9 min; 68% within 9 – 15 min; 68% – 90% over 15 – 16 min; 90% within 16 – 19 min and reset to 10% at 20 min. The spray voltage was 3.0 kV, and the cone voltage 35 V. The desolvation temperature was 413 K and source temperature 373 K. Nitrogen was used as both cone gas and desolvation gas with a flow rate of 40 L h^{-1} and 400 L h^{-1}, respectively. The collision energy was set up to 9.9 V. All spectra were acquired in the range of 100 – 2000 *m/z*. Data were collected and analyzed on a Mass Lynx (ver. 4.0).

X-ray crystallography

Single-crystal X-ray diffraction studies for 2-mercaptobenzanilide (**2**) and 2-phenyl-1,2-benzisothiazol-3(2*H*)-one (**4**) were carried out using graphite monochromated MoKα radiation (λ = 0.71073 Å) on a Rigaku Saturn 724 CCD area detector. The X-ray diffraction data of $[(\eta^6\text{-cym})Ru(en)(RS)]PF_6$ (**7**, R = $(C_6H_5)CONH(C_6H_5)$) were obtained on a Rigaku RA-Micro7HF diffractometer with Confocal Mo-Kα radiation (λ = 0.71073 Å) and $[((\eta^6\text{-cym})Ru)_2(RS)_3]PF_6$ (**8**) on a Rigaku R-AXIS RAPID diffractometer with graphite monochromated MoKα

radiation (λ= 0.71073 Å) on a Rigaku raxis Rapid IP Area Detector. All data were collected at 173 K, and structure solution and refinement were performed using the SHELXL-97. Standard data relating to the X-ray crystal structures of compounds **2**, **4**, **7** and **8** have been deposited in the Cambridge Crystallographic Data Centre with CCDC reference numbers 821489, 821490, 821491 and 821492, respectively.

PTP1B Inhibition Assay

Following a similar procedure to that described in the literuture,[52] the PTP1B activity was determined at 298 K in a reaction mixture (pH 7.2) containing 10 mM pNPP as substrate, 20 mM MOPS and 2 mM DTT. Inhibition assays were performed in the same buffer on a 96-well plate. Firstly, 10 μL of ruthenium complex **1** at various concentrations was mixed with 70 μL of enzyme in MOPS (20 mM) buffer (the final concentration of PTP1B was 250 nM), and the resulting mixture was incubated at 298 K for 30 min. Then 5 μL DTT was added and the mixture was incubated at 298 K for another 30 min to restore enzyme activity, and finally 10 μL of *p*NPP (0.02 M) substrate was added. After incubation for 30 min at 298 K, the enzymatic reactions were stopped by addition of 5 μL of 1 M NaOH, and the absorption was determined at 405 nm. Nonenzymatic hydrolysis of the substrate was corrected by measuring the control samples without addition of enzyme. IC_{50} values were generated by fitting the concentration-dependent inhibition curves using the program Origin (ver 7.5). All data points were obtained in sextuplicate.

Acknowledgements

We thank the NSFC (grant Nos: 90713020 , 20975103, 21005081 and 21020102039), the 973 Program of MOST (No: 2007CB935601), the Chinese Academy of Sciences (Hundred Talent Program), and the European Research Council (grant no. 247450) for support, and Dr. Maolin Guo of the University of Massachusetts Dartmouse for PTP1B.

Notes and References

[a] *Beijing National Laboratory for Molecular Sciences, The CAS Key Laboratory of Analytical Chemistry for Living Biosystems, Institute of Chemistry, Beijing, China. Tel: +86-10-62529069; E-mail: fuyi.wang@iccas.ac.cn*

[c] *Department of Chemistry, University of Warwick, Gibbet Hill Road, Coventry CV4 7AL, UK. Tel:+44-24-76523653; E-mail: P.J.Sadler@warwick.ac.uk*

†Electronic Supplementary Information (ESI) available: HPLC, UV-Vis and LC-ESI-MS data, Figure S1-S11. See DOI: 10.1039/b000000x/

1. P. C. A. Bruijnincx and P. J. Sadler, *Curr. Opin. Chem. Biol.*, 2008, **12**, 197.
2. P. C. A. Bruijnincx and P. J. Sadler, *Adv. Inorg. Chem.*, 2009, **61**, 1.
3. K. D. Camm, A. El-Sokkary, A. L. Gott, P. G. Stockley, T. Belyaeva and P. C. McGowan, *Dalton Trans.*, 2009, 10914.
4. C. G. Hartinger and P. J. Dyson, *Chem. Soc. Rev.*, 2009, **38**, 391.
5. B. T. Loughrey, P. C. Healy, P. G. Parsons and M. L. Williams, *Inorg. Chem.*, 2008, **47**, 8589.
6. E. Meggers, G. E. Atilla-Gokcumen, K. Grundler, C. Frias and A. Prokop, *Dalton Trans.*, 2009, 10882.
7. M. G. Mendoza-Ferri, C. G. Hartinger, R. E. Eichinger, N. Stolyarova, K. Severin, M. A. Jakupec, A. A. Nazarov and B. K. Keppler, *Organometallics*, 2008, **27**, 2405.
8. J. Ruiz, C. Vicente, C. de Haro and D. Bautista, *Dalton Trans.*, 2009, 5071.
9. C. Scolaro, A. Bergamo, L. Brescacin, R. Delfino, M. Cocchietto, G. Laurenczy, T. J. Geldbach, G. Sava and P. J. Dyson, *J. Med. Chem.*, 2005, **48**, 4161.
10. R. E. Aird, J. Cummings, A. A. Ritchie, M. Muir, R. E. Morris, H. Chen, P. J. Sadler and D. I. Jodrell, *Br. J. Cancer*, 2002, **86**, 1652.

11. R. E. Morris, R. E. Aird, P. D. Murdoch, H. M. Chen, J. Cummings, N. D. Hughes, S. Parsons, A. Parkin, G. Boyd, D. I. Jodrell and P. J. Sadler, *J. Med. Chem.*, 2001, **44**, 3616.

12. F. Y. Wang, A. Habtemariam, E. P. L. van der Geer, R. Fernandez, M. Melchart, R. J. Deeth, R. Aird, S. Guichard, F. P. A. Fabbiani, P. Lozano-Casal, I. D. H. Oswald, D. I. Jodrell, S. Parsons and P. J. Sadler, *Proc. Natl. Acad. Sci. U. S. A.*, 2005, **102**, 18269.

13. Y. K. Yan, M. Melchart, A. Habtemariam and P. J. Sadler, *Chem. Commun.*, 2005, 4764.

14. M. A. Bennett, M. J. Byrnes and I. Kovacik, *J. Organomet. Chem.*, 2004, **689**, 4463.

15. C. S. Allardyce, P. J. Dyson, D. J. Ellis and S. L. Heath, *Chem. Commun.*, 2001, 1396.

16. H. K. Liu, F. Y. Wang, J. A. Parkinson, J. Bella and P. J. Sadler, *Chem. Eur. J.*, 2006, **12**, 6151.

17. T. Bugarcic, O. Novakova, A. Halamikova, L. Zerzankova, O. Vrana, J. Kasparkova, A. Habtemariam, S. Parsons, P. J. Sadler and V. Brabec, *J. Med. Chem.*, 2008, **51**, 5310.

18. H. M. Chen, J. A. Parkinson, S. Parsons, R. A. Coxall, R. O. Gould and P. J. Sadler, *J. Am. Chem. Soc.*, 2002, **124**, 3064.

19. C. Gossens, I. Tavernelli and U. Rothlisberger, *J. Am. Chem. Soc.*, 2008, **130**, 10921.

20. A. Frodl, D. Herebian and W. S. Sheldrick, *J. Chem. Soc., Dalton Trans.*, 2002, 3664.

21. F. Y. Wang, H. M. Chen, J. A. Parkinson, P. D. Murdoch and P. J. Sadler, *Inorg. Chem.*, 2002, **41**, 4509.

22. F. Y. Wang, J. J. Xu, A. Habtemariam, J. Bella and P. J. Sadler, *J. Am. Chem. Soc.*, 2005, **127**, 17734.

23. W. B. Hu, Q. Luo, X. Y. Ma, K. Wu, J. A. Liu, Y. Chen, S. X. Xiong, J. P. Wang, P. J. Sadler and F. Y. Wang, *Chem. Eur. J.*, 2009, **15**, 6586.

24. S. Maity, S. Hattacharya and S. Chaudhury, *Chemosphere*, 2009, **77**, 319.

25. H. Petzold, J. J. Xu and P. J. Sadler, *Angew. Chem. Int. Ed.*, 2008, **47**, 3008.

26. A. Ishii, K. Komiya and J. Nakayama, *J. Am. Chem. Soc.*, 1996, **118**, 12836.

27. K. Goto, M. Holler and R. Okazaki, *J. Am. Chem. Soc.*, 1997, **119**, 1460.

28. A. Salmeen, J. N. Andersen, M. P. Myers, N. K. Tonks and D. Barford, *Mol. Cell*, 2000, **6**, 1401.

29. J. R. Wiener, J. A. Hurteau, B. J. M. Kerns, R. S. Whitaker, M. R. Conaway, A. Berchuck and R. C. Bast, *Am. J. Obstet. Gynecol.*, 1994, **170**, 1177.

30. J. R. Wiener, B. J. M. Kerns, E. L. Harvey, M. R. Conaway, J. D. Iglehart, A. Berchuck and R. C. Bast, *J. Natl. Cancer Inst.*, 1994, **86**, 372.

31. S. J. Liu, L. F. Zeng, L. Wu, X. Yu, T. Xue, A. M. Gunawan, Y. Q. Long and Z. Y. Zhang, *J. Am. Chem. Soc.*, 2008, **130**, 17075.

32. S. J. Liu, B. Zhou, H. Y. Yang, Y. T. He, Z. X. Jiang, S. Kumar, L. Wu and Z. Y. Zhang, *J. Am. Chem. Soc.*, 2008, **130**, 8251.

33. D. E. Moller, *Nature*, 2001, **414**, 821.

34. R. H. van Huijsduijnen, A. Bombrun and D. Swinnen, *Drug Discov. Today*, 2002, **7**, 1013.

35. R. H. van Huijsduijnen, W. H. B. Sauer, A. Bombrun and D. Swinnen, *J. Med. Chem.*, 2004, **47**, 4142.

36. M. Bentires-Alj and B. G. Neel, *Cancer Res.*, 2007, **67**, 2420.

37. A. Salmeen, J. N. Andersen, M. P. Myers, T. C. Meng, J. A. Hinks, N. K. Tonks and D. Barford, *Nature*, 2003, **423**, 769.

38. B. K. Sarma and G. Mugesh, *J. Am. Chem. Soc.*, 2007, **129**, 8872.

39. S. Sivaramakrishnan, K. Keerthi and K. S. Gates, *J. Am. Chem. Soc.*, 2005, **127**, 10830.

40. R. L. M. van Montfort, M. Congreve, D. Tisi, R. Carr and H. Jhoti, *Nature*, 2003, **423**, 773.

41. *The IC_{50} value of inhibition of complex **1** against PTP1B was determined with p-nitrophenyl phosphate (pNPP) as a substrate, details was described in the Experimental section. More deteils will be published elsewhere.* .

42. K. Waisser, M. Pesina, P. Holy, M. Pour, O. Bures, J. Kunes, V. Klimesova, V. Buchta, P. Kubanova and J. Kaustova, *Arch. Pharm.*, 2003, **336**, 322.

43. D. Barford, A. J. Flint and N. K. Tonks, *Science*, 1994, **263**, 1397.

44. Y. Bae, W. D. Jang, N. Nishiyama, S. Fukushima and K. Kataoka, *Mol. Biosyst.*, 2005, **1**, 242.

45. F. Y. Wang, S. Weidt, J. J. Xu, C. L. Mackay, P. R. R. Langridge-Smith and P. J. Sadler, *J. Am. Soc. Mass Spectrom.*, 2008, **19**, 544.

46. T. Sriskandakumar, H. Petzold, P. C. A. Bruijnincx, A. Habtemariam, P. J. Sadler and P. Kennepohl, *J. Am. Chem. Soc.*, 2009, **131**, 13355.

47. H. Petzold and P. J. Sadler, *Chem. Commun.*, 2008, 4413.

48. F. F. Prinsloo, J. J. Pienaar and R. Vaneldik, *J. Chem. Soc. Dalton Trans.*, 1995, 3581.

49. K. J. Barnham, M. I. Djuran, P. S. Murdoch, J. D. Ranford and P. J. Sadler, *Inorg. Chem.*, 1996, **35**, 1065.

50. R. Y. C. Shin, J. J. Vittal, Z. Y. Zhou, L. L. Koh and L. Y. Goh, *Inorg. Chim. Acta*, 2003, **352**, 220.

51. A. Correa, I. Tellitu, E. Dominguez and R. SanMartin, *Org. Lett.*, 2006, **8**, 4811.

52. J. Montalibet, K. I. Skorey and B. P. Kennedy, *Methods*, 2005, **35**, 2.

Table 1. Crystallographic data for 2-mercaptobenzanilide (**2**), 2-phenyl -1,2 –benzisothiazol-3(2H)-one (**4**), $[(\eta^6\text{-cym})Ru(en)(RS)]PF_6$ (**7**) and $[((\eta^6\text{-cym})Ru)_2(RS)_3]PF_6$ (**8**), R = $C_6H_5CONHC_6H_4$.

	2	**4**	**7**	**8**
Chemical formula	$C_{13}H_{11}NOS$	$C_{13}H_9NOS$	$C_{26}H_{34}PF_6N_3OSRuCl_2$	$C_{62}H_{70}PF_6N_3O_6S_3Ru_2$
Molar mass	229.29	227.27	753.56	1396.50
Crystal system	orthorhombic	monoclinic	triclinic	triclinic
Crystal size/mm	0.37×0.29×0.26	0.48×0.26×0.17	0.17×0.15×0.10	0.53×0.46×0.36
Space group	*P2(1)2(1)2(1)*	*P2(1)/c*	*P-1*	*P-1*
Crystal	Colorless/ block	Colorless/ block	Yellow/ block	Red/ block
a / Å	9.6385(19)	5.8793(12)	10.811(2)	11.0581(3)
b / Å	11.635(2)	14.397(3)	12.467(3)	15.6374(4)
c / Å	20.051(4)	12.316(3)	12.891(3)	17.9756(5)
α / deg	90.00	90.00	100.77(3)	84.0760(10)
β / deg	90.00	98.23(3)	109.54(3)	80.4740(10)
γ / deg	90.00	90.00	98.87(3)	88.8860
T / K	173(2)	173(2)	173(2)	173(2)
Z	8	4	2	2
μ / *mm* $^{-1}$	0.263	0.287	0.851	0.696
θ *range* / deg	2.17-27.48	3.29-27.49	1.71-27.46	2.03-27.46
F(000)	960	472	764	1432
Reflns collected	18364	7080	19247	25422
Indep. reflns	5149	2341	7124	13920
Refns obs.[$I > 2\sigma(I)$]	4983	2105	6774	13153
R [F > 4ó(F)]$^{[a]}$	0.0355	0.0457	0.0384	0.0478
$R_w^{[b]}$	0.0859	0.1173	0.0958	0.0922
GOF$^{[c]}$	1.077	1.120	1.084	1.289
$\triangle\rho$ max and min [e Å^{-3}]	+0.209, -0.185	+0.284, -0.248	+0.681, -0.688	+0.733, -0.800

[a] $R = \sum||F_o| - |F_c||/\sum|F_o|$. [b] $R_w = [\sum w(F_o^2 - F_c^2)^2/\sum wF_o^2)]^{1/2}$. [c] GOF = $[\sum w(F_o^2 - F_c^2)^2/(n - p)]^{1/2}$, where n = number of reflections and *p* = number of parameters.

Table 2 Selected bond lengths (Å) and angles (°) for 2-mercaptobenzanilide (**2**), 2-phenyl-1,2–benzisothiazol -3(2*H*)-one (**4**). For numbering schemes see Figure 1.

2		**4**	
S1-C6	1.7650(17)	S1-C7	1.739(2)
C1-C6	1.398(2)	S1-N1	1.7186(16)
C5-C6	1.405(2)	N1-C8	1.430(2)
C4-C5	1.401(2)	N1-C1	1.380(2)
C5-C7	1.495(2)	O1-C1	1.222(2)
O1-C7	1.234(2)	C1-C2	1.467(3)
N1-C7	1.349(2)	C2-C3	1.393(3)
N1-C8	1.424(2)	C8-C9	1.390(3)
C6-S1-H1	97.80	C6-C7-S1	127.70(16)
S1-C6-C5	120.78(13)	C7-S1-N1	90.45(8)
C6-C5-C7	121.23(15)	C8-N1-S1	119.23(12)
C5-C7-O1	121.60(15)	C1-N1-S1	116.08(13)
O1-C7-N1	122.66(16)	N1-C1-O1	123.79(17)
C7-N1-C8	124.65(15)	C1-N1-C8	124.58(15)
N1-C8-C9	118.70(16)	N1-C1-C2	108.30(16)
N1-C8-C13	121.17(16)	O1-C1-C2	127.89(17)

Table 3 Positive ions observed by HPLC-ESI-MS from reaction mixtures of 2-mercaptobenzanilide (**2**) and H_2O_2, and Ru(II) arene thiolato complex $[(\eta^6\text{-cym})Ru(en)(RS)]PF_6$ (**7**) with H_2O_2 and GSH at 298 K, R = $C_6H_5CONHC_6H_4$. For chemical structures of observed ions see Schemes 1-5.

Reaction	pH	Reaction Time / h	RT[a] / min	Observed Ion	Obs (Calcd)[b] *m/z*
2 + H_2O_2, 1:1.4 mM	7.4	<0.5 h	10.95	[**2** + H[c]]$^+$	230.02(230.06)
			13.78	[**3** + H]$^+$	457.01(457.10)
		24 h	5.03	[**5** + H]$^+$	278.02(278.05)
			5.57	[**6** + H]$^+$	244.01(244.04)
			10.95	[**4** + H]$^+$	228.00(228.05)
			13.78	[**3** + H]$^+$	457.01(457.10)
7 + H_2O	7.4	60 h	5.02	[**1**-H_2O – H]$^+$	294.18 (294.07)
			8.56	[**7** – en]$^+$	464.20(464.07)
			11.03	[**2** + H]$^+$	230.02(230.06)
	5.3	60 h	8.56	[**7** – en]$^+$	464.20(464.07)
			10.71	[**9** – $2H_2O$]$^+$	464.20 (464.07)
7 + H_2O_2, 1:1.4 mM	7.4	72 h	5.05[d]	{**10**– (η^6-cym)}$^+$	422.16 (422.01)
				{**11** – en – H}$^+$	463.17 (463.07)
			5.57	[**6** + H]$^+$	244.01 (244.04)
			8.56	{**7** – en}$^+$	464.20 (464.07)
			10.95	[**4** + H]$^+$	228.00 (228.05)
	5.3	72 h	5.05[d]	{**10** – (η^6-cym)}$^+$	422.16 (422.01)
				{**11** – en – H}$^+$	463.17 (463.07)
			8.56	{**7** – en}$^+$	464.20 (464.07)
			10.71	[**9** – $2H_2O$]$^+$	464.20 (464.07)
			10.95	[**4** + H]$^+$	228.00 (228.05)
7 + H_2O_2 + GSH,[e] 1:1.4:10 mM	7.4	72 h	4.79	[**13** + H]$^{2+}$	695.64 (695.63)
			5.05[d]	{**10** – (η^6-cym)}$^+$	422.16 (422.01)
				{**11** – en – H}$^+$	463.17 (463.07)
			5.31	[**17**[f] + H]$^+$	535.21 (535.13)
			5.57	[**6** + H]$^+$	244.01 (244.04)
			8.56	{**7** –en}$^+$	464.20 (464.07)
			11.03	[**2** + H]$^+$	230.02 (230.06)

7 + GSH, 1:10 mM	7.4	72 h	4.79	{**12** – en – Glu}$^{+}$	413.17(413.05)
			8.56	{**7** – en}$^{+}$	464.20 (464.07)
			11.03	[**2** + H]$^{+}$	230.02 (230.06)
	5.3	72 h	4.79	[**13** + H]$^{2+}$	695.64 (695.63)
			5.07	[**14** + H]$^{2+}$	656.89 (656.62)
			8.56	{**7** – en}$^{+}$	464.20 (464.07)
			10.56	[**15** + H]$^{2+}$	617.35 (617.61)
			11.03	[**2** + H]$^{+}$	230.02 (230.06)
			11.81	[**16**^{g} + H]$^{+}$	1053.21(1053.09)

[a] RT is the retention time of detected compounds in HPLC traces (Figures 2, 4, 5, 6 and S4).

[b] Observed (Obs) and calculated (Calcd) mass-to-charge ratios for the most abundant iostope of observed ions. For mass spectra see Figures S1-S4 and S6-S7.

[c] H indicates gain (+) or loss (-) of a proton.

[d] The fraction contains a mixture of products **10** and **11**.

[e] Complex **7** firstly reacted with with H_2O_2 for 24 h and then added GSH into the reaction mixture for further reaction for 72 h after removing excess of H_2O_2 by addition of catalase.

[f] **17** = RS-SG, R = $C_6H_5CONHC_6H_4$.

[g] **16** = [((η^6-cym)Ru)$_2$(RS)$_2$(CHCO$_2$)(PO$_3$)].

Table 4 Selected bond lengths (Å) and angles (°) for $[(\eta^6\text{-cym})Ru(en)(RS)]PF_6$ (**7**) and $[((\eta^6\text{-cym})Ru)_2(RS)_3]PF_6$ (**8**), R = $C_6H_5CONHC_6H_4$. For numbering schemes see Figure 3.

7		**8**			
Ru-N3	2.128(2)	Ru1-S1	2.4077(7)	Ru2-S1	2.3916(7)
Ru-N2	2.147(2)	Ru1-S2	2.3940(7)	Ru2-S2	2.4163(7)
Ru-S1	2.4059(9)	Ru1-S3	2.4015(7)	Ru2-S3	2.4068(7)
Ru-C16	2.202(3)	Ru1-C1	2.248(3)	Ru2-C11	2.212(3)
Ru-C17	2.209(3)	Ru1-C2	2.213(3)	Ru2-C12	2.210(3)
Ru-C18	2.178(3)	Ru1-C3	2.215(3)	Ru2-C13	2.194(3)
Ru-C19	2.201(3)	Ru1-C4	2.236(3)	Ru2-C14	2.227(3)
Ru-C20	2.169(3)	Ru1-C5	2.211(3)	Ru2-C15	2.207(3)
Ru-C21	2.177(3)	Ru1-C6	2.190(3)	Ru2-C16	2.219(3)
Ru-cent[a]	1.6688(4)	Ru1- cent[a]	1.7068(2)	Ru2- cent[a]	1.6956(2)
N3-Ru1-N2	78.87(9)	C21-S1-Ru1	112.14(10)	C21-S1-Ru2	115.84(10)
N2-Ru1-S1	83.68(7)	C34-S2-Ru1	111.82(10)	C34-S2-Ru2	112.22(9)
N3-Ru1-S1	84.16(7)	C47-S3-Ru1	114.80(10)	C47-S3-Ru2	106.64(9)

[a] Cent = centroid of η^6-*p*-cymene

Scheme 1 Pathways for the redox reactions and cyclization of model compound **2** with H_2O_2 and GSH in phosphate buffer (pH 7.4).

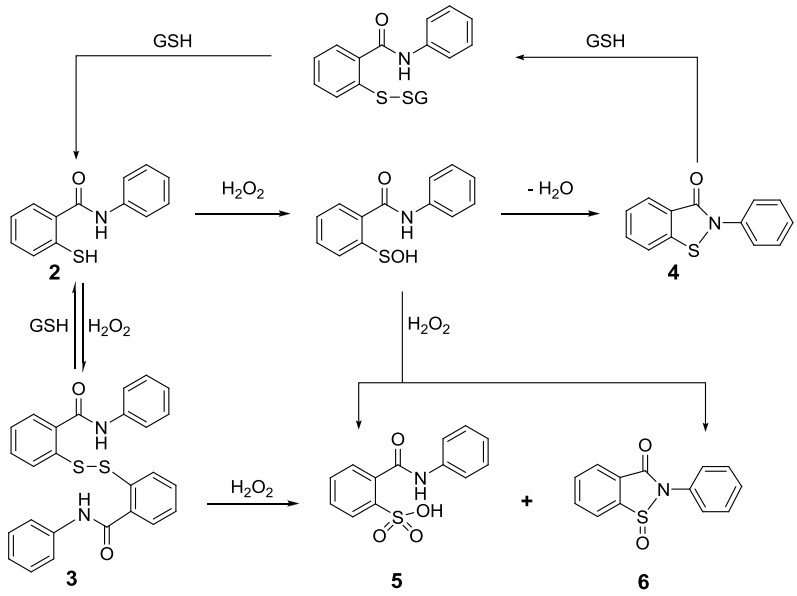

Scheme 2 Pathways for reactions of complex **1** with model compound **2** in phosphate buffer.

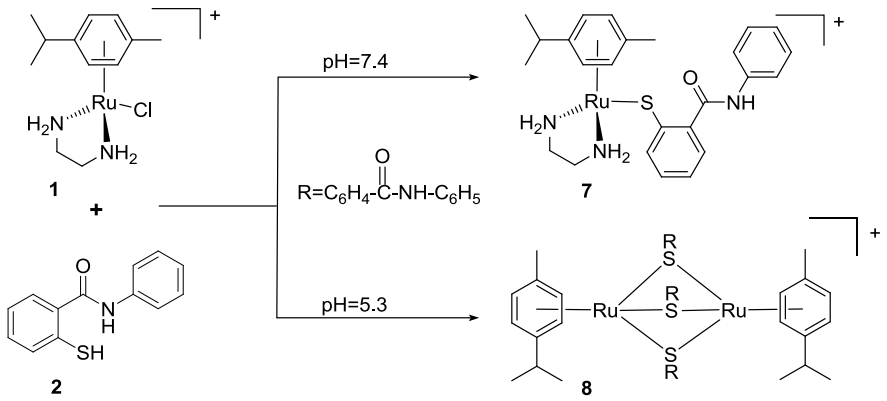

Scheme 3 Pathways for the hydrolysis of complex **7** in phosphate buffer. At pH 7.4, complex **7** undergoes slow hydrolysis, giving rise to a minor amount of the aqua product 1-H_2O.

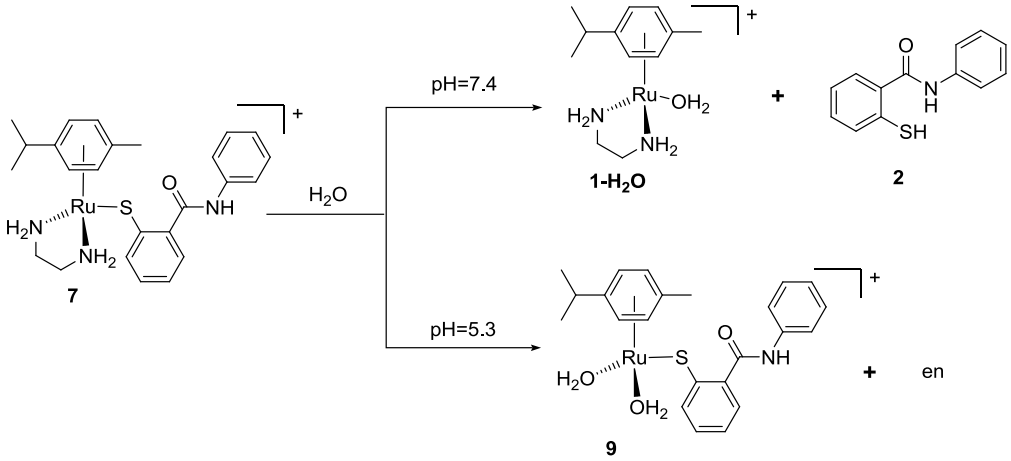

Scheme 4 Pathways for the reaction of complex **7** with hydrogen peroxide in phosphate buffers of pH 7.4 or 5.3.

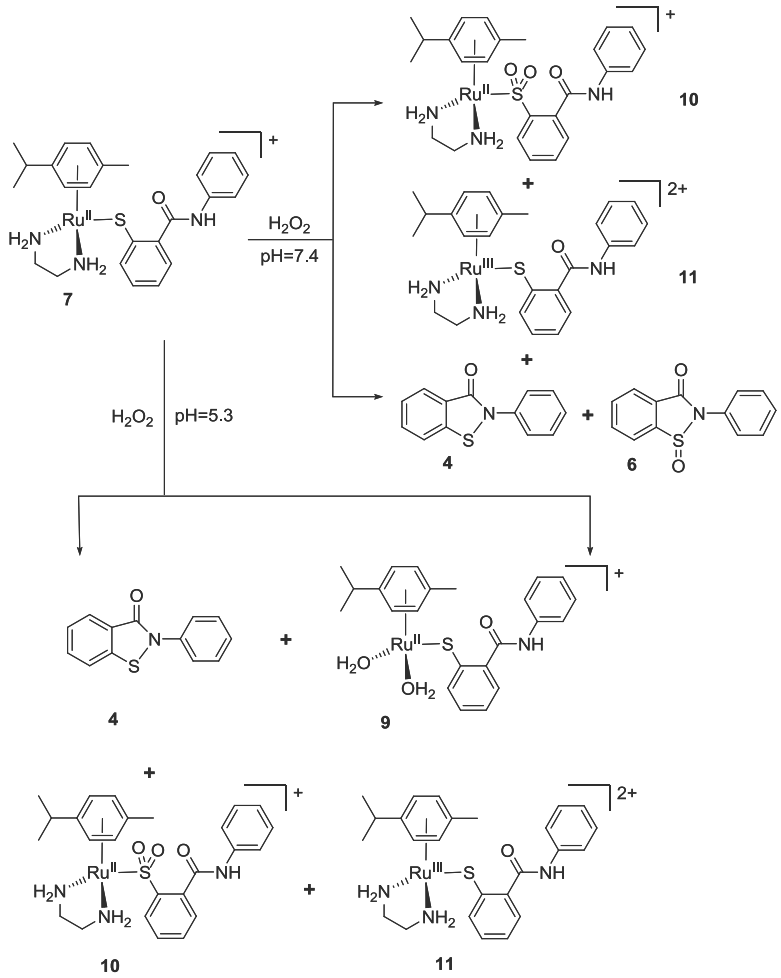

Scheme 5 Pathways for reactions of complex **7** with GSH in different pH of phosphate buffer. The formate and phosphate ligands in adduct **16** come from the HPLC solvents and the phosphate buffer, respectively.

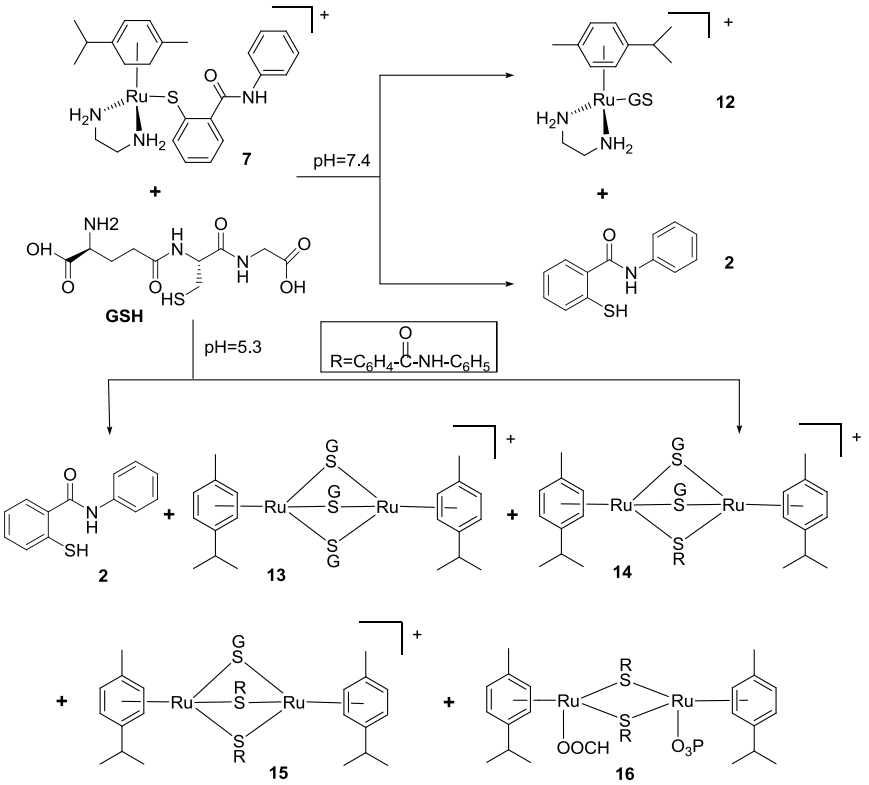

Figure Captions

Fig. 1. X-ray crystal structures and atom numbering schemes for a) 2-mercaptobenzanilide (**2**), and b) 2-phenyl-1,2-benzisothiazol-3(2H)-one (**4**) at 50% probability thermal ellipsoids.

Fig. 2. a) HPLC time-course for the reaction of compound **2** (1 mM) with 1.4 mol equiv H_2O_2 in 50 mM phosphate buffer (pH 7.4) at 298 K. Peak assignments: a, **2**; b, **3**; c, **4**; d, **5** and e, **6**. The chemical structures of oxidized products **3** – **6** are shown in Scheme 1. b) UV-Vis spectra of HPLC fractions a (solid line) and c (dashed line) in (a) from the reaction mixtures of compound **2** with H_2O_2. Mass spectra for all fractions are shown in Figure S1.

Fig. 3. X-ray crystal structure and atom numbering scheme for the cation of $[(\eta^6\text{-cym})Ru(en)(RS)]PF_6$ (**7**) at 50% probability thermal ellipsoids

Fig. 4. Two views of the X-ray crystal structure of the dinuclear cation of $[((\eta^6\text{-cym})Ru)_2(RS)_3]PF_6$ (**8**) at 20% probability thermal ellipsoids, together with the atom numbering scheme.

Fig. 5. HPLC time-courses for the reactions of a) thiolato complex **7** (1 mM) with 1.4 mol equiv. H_2O_2 in 50 mM phosphate buffer (pH 7.4) at 298 K, and b) complex **7** (1 mM), which has reacted with 1.4 mol equiv. H_2O_2 in phosphate buffer (pH 7.4) at 298 K for 24 h, with 10 mol equiv. GSH after removing excess of H_2O_2 using catalase. The inset g indicates that the shoulder on peak h contains a mixture of two adducts as evidenced by the distinct UV-Vis spectra corresponding to fractions eluting at 5.00 and 5.05 min shown in Figure S5. Peak assignments: a, **2**; c, **4**; e, **6**; f, $\mathbf{7}^+$; h, $\mathbf{10}^+$ and $\mathbf{11}^{2+}$; i, $\mathbf{13}^{2+}$ and j, **17**. Mass spectra for all fractions in this figure are shown in Figures S6 and S8.

Fig. 6. HPLC time-courses for the reaction of thiolato complex **7** (1 mM) with 1.4 mol equiv H_2O_2 in 50 mM phosphate buffer at pH 5.3 and at 298 K. The inset h indicates that with a shoulder peak h contains a mixture of two adducts as evidenced by the distinct UV-Vis spectra corresponding to fractions eluting at 5.00 and 5.05 min shown in Figure S5. Peak assignments: c, **4**; e, **6**; f, $\mathbf{7}^+$; g, $\mathbf{9}^+$; and h, $\mathbf{10}^+$ and $\mathbf{11}^{2+}$. Mass spectra for all fractions are shown in Figure S9.

Fig. 7. HPLC time-courses for the reactions of **7** (1 mM) with 10 mol equiv GSH in 50 mM phosphate buffer at a) pH 7.4 and b) pH 5.3 and at 298 K. Peak assignments: a, **2**; f, $\mathbf{7}^+$; k, $\mathbf{12}^+$; i, $\mathbf{13}^+$; l, $\mathbf{14}^+$; m, $\mathbf{15}^+$ and n, **16**. Mass spectra for all fractions in this figure are shown in Figures S10 and S11.

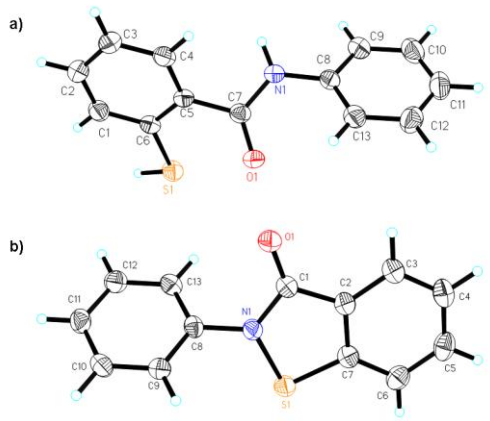

Fig. 1. X-ray crystal structures and atom numbering schemes for a) 2-mercaptobenzanilide (**2**), and b) 2-phenyl-1,2-benzisothiazol-3(2H)-one (**4**) at 50% probability thermal ellipsoids.

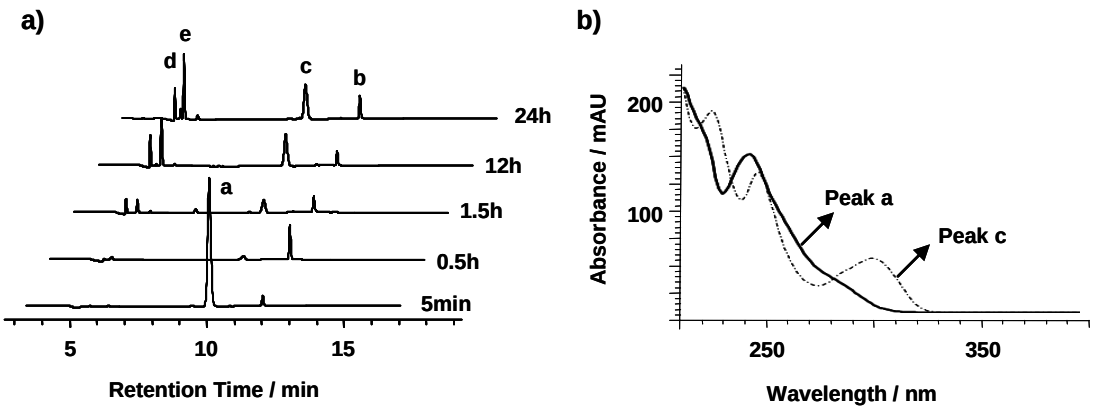

Fig. 2. a) HPLC time-course for the reaction of compound **2** (1 mM) with 1.4 mol equiv H_2O_2 in 50 mM phosphate buffer (pH 7.4) at 298 K. Peak assignments: a, **2**; b, **3**; c, **4**; d, **5** and e, **6**. The chemical structures of oxidized products **3** – **6** are shown in Scheme 1. **b)** UV-Vis spectra of HPLC fractions a (solid line) and c (dashed line) in (a) from the reaction mixtures of compound **2** with H_2O_2. Mass spectra for all fractions are shown in Figure S1.

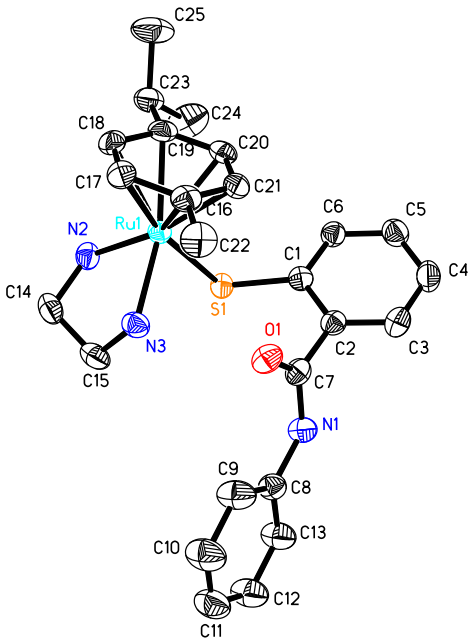

Fig. 3. X-ray crystal structure and atom numbering scheme for the cation of $[(\eta^6\text{-cym})Ru(en)(RS)]PF_6$ (**7**) at 50% probability thermal ellipsoids.

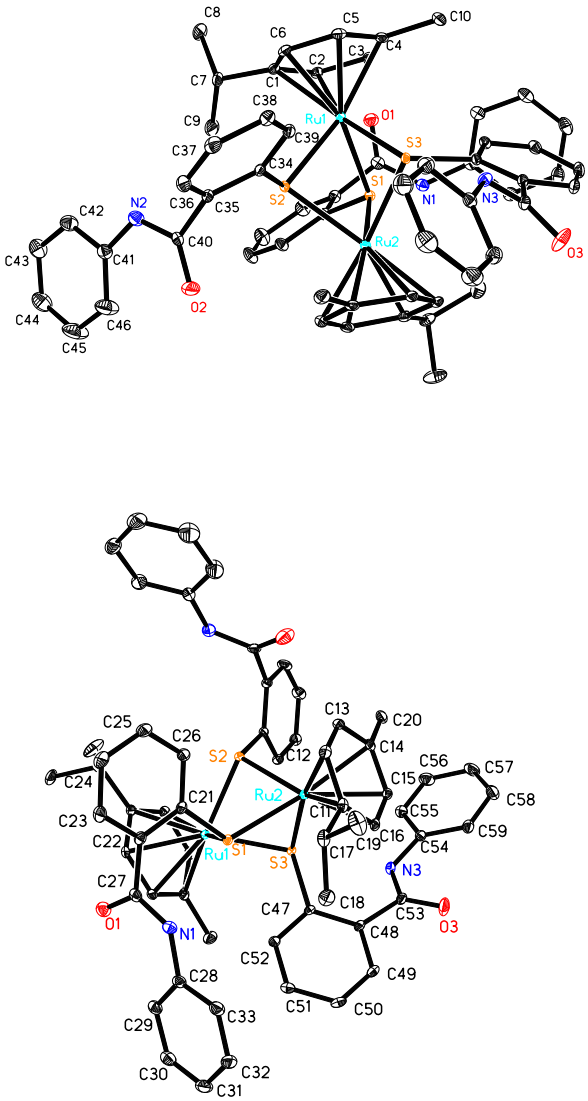

Fig. 4. Two views of the X-ray crystal structure of the dinuclear cation of $[((\eta^6\text{-cym})Ru)_2(RS)_3]PF_6$ (**8**) at 20% probability thermal ellipsoids, together with the atom numbering scheme.

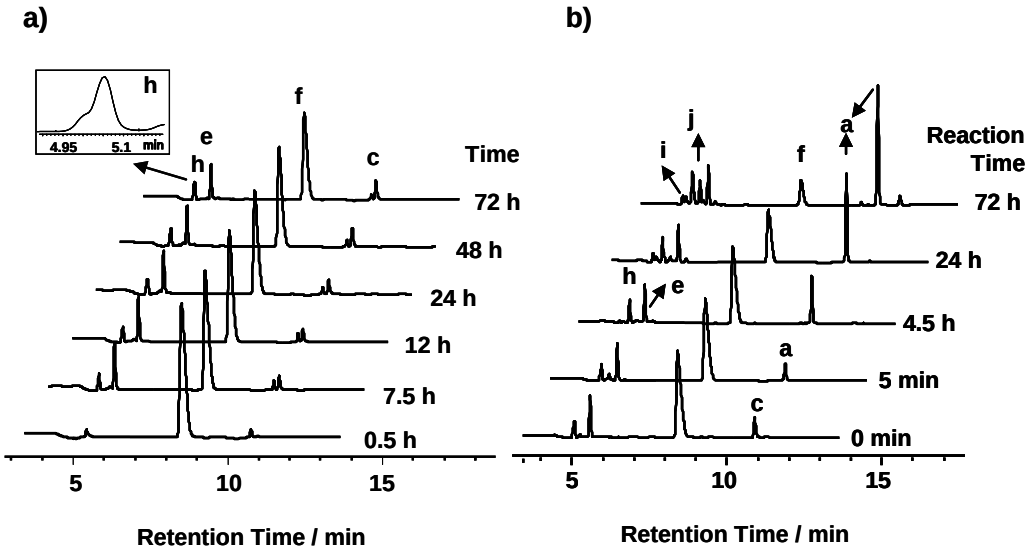

Fig. 5. HPLC time-courses for the reactions of a) thiolato complex **7** (1 mM) with 1.4 mol equiv. H_2O_2 in 50 mM phosphate buffer (pH 7.4) at 298 K, and b) complex **7** (1 mM), which has reacted with 1.4 mol equiv. H_2O_2 in phosphate buffer (pH 7.4) at 298 K for 24 h, with 10 mol equiv. GSH after removing excess of H_2O_2 using catalase. The inset g indicates that the shoulder on peak h contains a mixture of two adducts as evidenced by the distinct UV-Vis spectra corresponding to fractions eluting at 5.00 and 5.05 min shown in Figure S5. Peak assignments: a, **2**; c, **4**; e, **6**; f, $\mathbf{7}^{+}$; h, $\mathbf{10}^{+}$ and $\mathbf{11}^{2+}$; i, $\mathbf{13}^{2+}$ and j, **17**. Mass spectra for all fractions in this figure are shown in Figures S6 and S8.

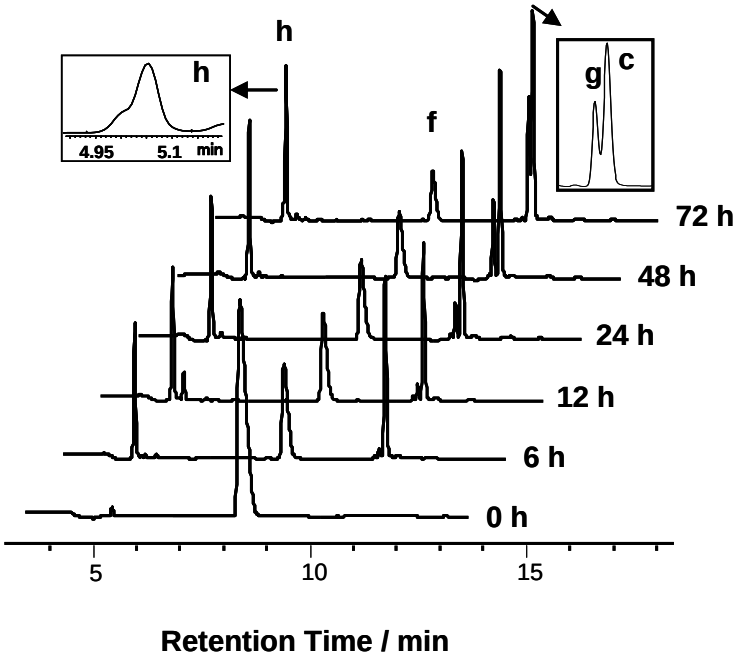

Fig. 6. HPLC time-courses for the reaction of thiolato complex **7** (1 mM) with 1.4 mol equiv H_2O_2 in 50 mM phosphate buffer at pH 5.3 and at 298 K. The inset h indicates that with a shoulder peak h contains a mixture of two adducts as evidenced by the distinct UV-Vis spectra corresponding to fractions eluting at 5.00 and 5.05 min shown in Figure S5. Peak assignments: c, **4**; e, **6**; f, $\mathbf{7}^+$; g, $\mathbf{9}^+$; and h, $\mathbf{10}^+$ and $\mathbf{11}^{2+}$. Mass spectra for all fractions are shown in Figure S9.

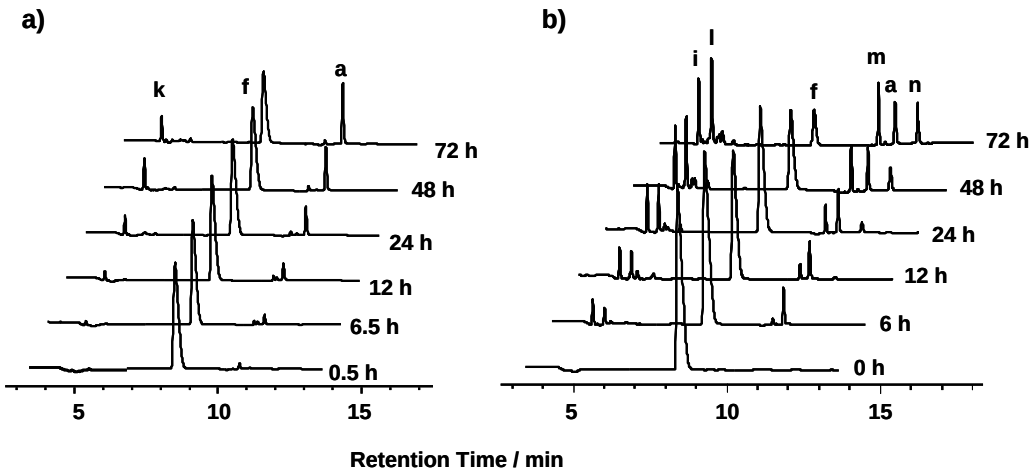

Fig. 7. HPLC time-courses for the reactions of **7** (1 mM) with 10 mol equiv GSH in 50 mM phosphate buffer at a) pH 7.4 and b) pH 5.3 and at 298 K. Peak assignments: a, **2**; f, $\mathbf{7}^+$; k, $\mathbf{12}^+$; i, $\mathbf{13}^+$; l, $\mathbf{14}^+$; m, $\mathbf{15}^+$ and n, **16**. Mass spectra for all fractions in this figure are shown in Figures S10 and S11.